Hybrid Precoding and Channel Estimation

A Project Report

submitted by

KARTHIK SURESH

in partial fulfilment of the requirements
for the award of the degree of

DUAL DEGREE (B.Tech. and M.Tech.)

DEPARTMENT OF ELECTRICAL ENGINEERING
INDIAN INSTITUTE OF TECHNOLOGY MADRAS.

JUNE 2021

THESIS CERTIFICATE

This is to certify that the thesis titled **Hybrid Precoding and Channel Estimation**, submitted by **Karthik Suresh**, to the Indian Institute of Technology, Madras, for the award of the degree of **Dual Degree (B.Tech + M.Tech)**, is a bona fide record of the research work done by him under our supervision. The contents of this thesis, in full or in parts, have not been submitted to any other Institute or University for the award of any degree or diploma.

Prof. Srikrishna Bhashyam
Research Guide
Professor
Dept. of Electrical Engineering
IIT Madras, 600 036

Place: Chennai

Date:

ACKNOWLEDGEMENTS

I would like to thank Prof. Srikrishna Bhashyam for guiding me through the project and his constant help and support. I would like to thank all my professors at IITM for helping me through my journey at IIT Madras. I would also like to thank my parents, my sister and all my friends for their constant support.

ABSTRACT

KEYWORDS: Hybrid Precoding, mmWave, MIMO, OMP, Alternating Minimization, Double Phase Shifter, Fixed Phase Shifter, Channel Estimation

We understand the hybrid precoding problem for mmWave MIMO systems and look at algorithms and hardware implementations for the same. We perform simulations to replicate/verify the results shown in these papers. We then consider the channel estimation problem for hybrid precoding and try to compare some of the hybrid precoding algorithms in this scenario through simulations.

TABLE OF CONTENTS

LIST OF FIGURES

CATEGORIZATION OF FIGURES

- **Figures from papers** - 1.13, 1.15, 1.17, 2.6
- **Figures using algorithms found online** - 1.8, 1.9, 1.16
- **Figures using our own simulations** - 1.4, 1.5, 1.14, 2.4, 2.5

ABBREVIATIONS

AoA	Angle of Arrival
AoD	Angle of Departure
BS	Base Station
CSI	Channel State Information
DPS	Double Phase Shifter
FPS	Fixed Phase Shifter
MIMO	Multiple Input Multiple Output
mmWave	Millimeter Wave
MO	Manifold Optimization
MS	Mobile Station
MU	Multiple User
OMP	Orthogonal Matching Pursuit
PE	Phase Extraction
SDR	Semi-Definite Relaxation
SPS	Single Phase Shifter
SU	Single user

CHAPTER 1

HYBRID PRECODING

1.1 Introduction

Millimeter wave (mmWave) communication has enabled increased data rates and system capacities with the use of multiple antennas. The higher frequencies lead to a significant increase in free-space path loss but this can be compensated by a large antenna array which is enabled by the decreased size of antennas at higher frequencies. It also enables the use of spatial multiplexing, i.e. transmitting multiple data streams which increases the spectral efficiency.

The increased number of antenna elements also leads to an increase in power consumption and implementation cost due to a proportional increase in digital hardware to achieve capacity. This has led to mmWave systems relying heavily on analog/RF components like phase shifters or switches. However, analog processing places a constant modulus constraint on the precoding matrix which limits the rates achievable. Further, analog beamforming only supports single stream transmission, and cannot fully exploit the available spatial resource. This has motivated the exploration of hybrid precoding schemes which use both analog and digital components. The RF chains connect a low dimensional digital precoder to the antennas through phase shifters resulting in a high dimensional hybrid precoder.

In the following sections, we discuss the Orthogonal Matching Pursuit algorithm proposed in "Spatially sparse precoding in millimeter wave mimo systems" (Ayach *et al.*, 2014), the Alternating Minimization algorithms proposed in "Alternating minimization algorithms for hybrid precoding in millimeter wave mimo systems" (Yu *et al.*, 2016) and the new hardware architechtures and algorithms proposed in "Hybrid beamforming for 5g and beyond millimeter-wave systems: A holistic view "(Zhang *et al.*, 2020) and perform simulations for the same.

The notation used in this and the following chapter is listed below for convenience. We use $\mathbf{A}$ to denote a matrix; $\mathbf{a}$ for a column vector; a to denote a scalar; $\mathbf{A}^H$ for the

conjugate transpose (hermitian) of $\mathbf{A}$; $\mathbf{A}^T$ for the transpose of $\mathbf{A}$; $\mathbf{A}^*$ for the conjugate of $\mathbf{A}$; $\mathbf{A}^\dagger$ for the Moore-Penrose pseudo-inverse of $\mathbf{A}$. $|\mathbf{A}|$ and $\|\mathbf{A}\|_F$ denote the determinant and Frobenius norm of $\mathbf{A}$. $[\mathbf{A}|\mathbf{B}]$ denotes horizontal concatenation of matrices; $diag(\mathbf{A})$ denotes the vector of diagonal elements of $\mathbf{A}$; $tr(\mathbf{A})$ denotes the trace of $\mathbf{A}$; I_N denotes the $N \times N$ identity matrix. $\mathbb{E}[\cdot]$ denotes expectation and $\Re$ denotes the real part.

1.2 Orthogonal Matching Pursuit

1.2.1 System model

We consider the single-user mmWave system as shown in figure 1.1 with N_t transmit antennas, N_r receive antennas and N_s data streams. The hybrid architecture on the transmitter side consists of N_t^{RF} ($N_s \leq N_t^{RF} \leq N_t$) transmit RF chains which connect the digital baseband precoder $\mathbf{F}_{\text{BB}}$ of dimension $N_t^{RF} \times N_s$ to the transmit antennas through phase shifters. The phase shifters are denoted by the RF precoder $\mathbf{F}_{\text{RF}}$ of dimension $N_t \times N_t^{RF}$. The transmitted signal is thus given by $\mathbf{x} = \mathbf{F}_{\text{RF}}\mathbf{F}_{\text{BB}}\mathbf{s}$, where $\mathbf{s}$ is the $N_s \times 1$ symbol vector.

The constraints on the precoder are as follows. Since $\mathbf{F}_{\text{RF}}$ is implemented using RF components, we place a constant norm constraint on its elements. Further, the total transmit power constraint is imposed as $\|\mathbf{F}_{\text{RF}}\mathbf{F}_{\text{BB}}\|_F^2 = N_s$.

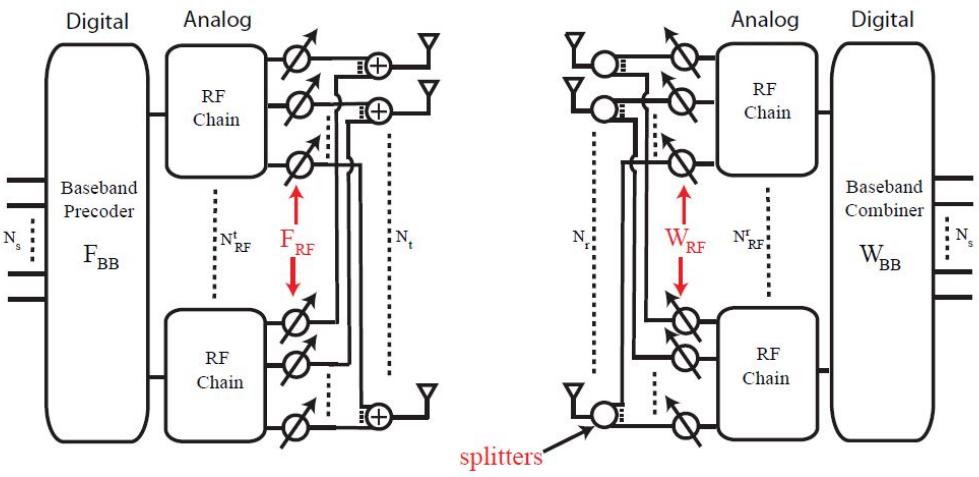

Figure 1.1: SU-MIMO system with Hybrid precoding (Ayach *et al.* (2014))

We consider a narrowband block-fading propagation channel with channel matrix $\mathbf{H}$ of dimension $N_r \times N_t$. Thus, the received signal is written as

$$\mathbf{y} = \sqrt{\rho}\mathbf{H}\mathbf{F}_{\text{RF}}\mathbf{F}_{\text{BB}}\mathbf{s} + \mathbf{n} \tag{1.1}$$

where $\mathbf{y}$ is the $N_r \times 1$ received vector, ρ is the averaged receive power and $\mathbf{n}$ is the vector of i.i.d. $\mathcal{CN}(0, \sigma_n^2)$ noise. Note that we assume perfect CSI at both the transmitter and receiver for this chapter. We will look at the performance of these precoding schemes under imperfect CSI in the next chapter.

The receiver structure is similar to the transmitter one with phase shifters passing the signal into N_r^{RF} ($N_s \leq N_r^{RF} \leq N_r$) RF chains. The received signal is passed through the RF combiner $\mathbf{W}_{\text{RF}}$ and Baseband combiner $\mathbf{W}_{\text{BB}}$ to obtain the processed received signal

$$\tilde{\mathbf{y}} = \sqrt{\rho}\mathbf{W}_{\text{BB}}^H\mathbf{W}_{\text{RF}}^H\mathbf{H}\mathbf{F}_{\text{RF}}\mathbf{F}_{\text{BB}}\mathbf{s} + \mathbf{W}_{\text{BB}}^H\mathbf{W}_{\text{RF}}^H\mathbf{n}. \tag{1.2}$$

The achievable spectral efficiency when gaussian symbols are transmitted over the mmWave channel is given by

$$R = \log_2\left(\left|\mathbf{I}_{N_s} + \frac{\rho}{\sigma_N^2 N_s}(\mathbf{W}_{\text{RF}}\mathbf{W}_{\text{BB}})^\dagger\mathbf{H}\mathbf{F}_{\text{RF}}\mathbf{F}_{\text{BB}}\mathbf{F}_{\text{BB}}^H\mathbf{F}_{\text{RF}}^H\mathbf{H}^H\mathbf{W}_{\text{RF}}\mathbf{W}_{\text{BB}}\right|\right) \tag{1.3}$$

1.2.2 Channel model

We consider the clustered channel model based on the Saleh-Valenzuela model (Rappaport *et al.* (2015)). The channel matrix H is written as

$$\mathbf{H} = \gamma\sum_{i=1}^{N_{cl}}\sum_{l=1}^{N_{ray}}\alpha_{il}\mathbf{a_r}(\phi_{il}^r, \theta_{il}^r)\mathbf{a_t}(\phi_{il}^t, \theta_{il}^t)^H \tag{1.4}$$

where $\gamma = \sqrt{N_t N_r / N_{cl} N_{ray}}$ is a normalization factor, N_{cl} and N_{ray} represent the number of clusters and the number of rays in each cluster, and α_{il} denotes the gain of the lth ray in the ith scattering cluster. $\phi_{il}^r(\theta_{il}^r)$ and $\phi_{il}^t(\theta_{il}^t)$ are the azimuth (elevation) angles of arrival (AoAs) and departure (AoDs) respectively. We consider α_{il} to be i.i.d.

$\mathcal{CN}(0, \sigma^2_{\alpha,i})$ distributed where $\sigma^2_{\alpha,i}$ is the average cluster power of the ith cluster and $\sum_{i=1}^{N_{cl}} \sigma^2_{\alpha,i} = \gamma$.

We consider the N_{ray} azimuth and elevation angles of departure and arrival to follow a Laplacian distribution with a uniformly random mean cluster angle of ϕ_i and θ_i respectively and a constant angular spread. For the purpose of simulations, we consider the array response vectors $\mathbf{a_r}(\phi^r_{il}, \theta^r_{il})$ and $\mathbf{a_t}(\phi^t_{il}, \theta^t_{il})$ to follow a Uniform Planar Array (UPA) structure with $\sqrt{N} \times \sqrt{N}$ antennas where the array response vectors are as below:

$$\mathbf{a}(\phi_{il}, \theta_{il}) = \frac{1}{\sqrt{N}}\big[1, ..., e^{j\frac{2\pi}{\lambda}d(psin(\phi_{il})sin(\theta_{il})+qcos(\theta_{il}))}, \\ ..., e^{j\frac{2\pi}{\lambda}d((\sqrt{N}-1)sin(\phi_{il})sin(\theta_{il})+(\sqrt{N}-1)cos(\theta_{il}))}\big]^T \tag{1.5}$$

where λ is the signal wavelength and d is the antenna spacing; $0 \leq p < \sqrt{N}$ and $0 \leq q < \sqrt{N}$ are the antenna indices in the 2D plane.

Uniform planar arrays allow us to pack more antenna elements in a smaller area and thus lead to a higher beamforming gain per unit area.

1.2.3 Problem formulation and Orthogonal Matching Pursuit

We look at the approach taken by the authors briefly in this section and explain the Orthogonal Matching Pursuit algorithm for hybrid precoding. The task of maximizing the rate is a joint optimization over four matrix variables $(\mathbf{F}_{\text{RF}}, \mathbf{F}_{\text{BB}}, \mathbf{W}_{\text{RF}}, \mathbf{W}_{\text{BB}})$. We thus decouple the transmitter and receiver optimizations and design $\mathbf{F}_{\text{RF}}\mathbf{F}_{\mathbf{textBB}}$ to maximize the mutual information achieved by Gaussian signaling over the mmWave channel as stated below:

$$(\mathbf{F}^{\text{opt}}_{\text{RF}}, \mathbf{F}^{\text{opt}}_{\text{BB}}) = \underset{\mathbf{F}_{\text{BB}}, \mathbf{F}_{\text{RF}}}{\text{argmax}} \quad \mathcal{I}(\mathbf{F}_{\text{RF}}, \mathbf{F}_{\text{BB}}), \tag{1.6}$$
$$\text{s.t.} \quad \mathbf{F}_{\text{RF}} \in \mathcal{F}_{\text{RF}},$$
$$\|\mathbf{F}_{\text{RF}}\mathbf{F}_{\text{BB}}\|^2_F = N_s$$

where $\mathcal{F}_{\text{RF}}$ is the set of feasible RF precoders, i.e., the set of $N_t \times N_t^{\text{RF}}$ matrices with constant-magnitude entries. The authors rewrite equation 1.6 in terms of the distance between $\mathbf{F}_{\text{RF}}\mathbf{F}_{\text{BB}}$ and the optimal digital precoder $\mathbf{F}_{\text{opt}}$. This is done by writing the channel matrix using its singular value decomposition (SVD) - $\mathbf{H} = \mathbf{U}\mathbf{\Sigma}\mathbf{V}^H$, where $\mathbf{U}$ is a $N_r \times N_r$ unitary matrix, $\mathbf{\Sigma}$ is a $N_r \times N_t$ diagonal matrix with rank equal to the rank of $\mathbf{H}$ and $\mathbf{V}$ is a $N_t \times N_t$ unitary matrix. It is shown that the optimal precoding matrix is the first N_s columns of $\mathbf{V}$. The precoder design problem is rewritten as

$$\begin{aligned}(\mathbf{F}_{\text{RF}}^{\text{opt}}, \mathbf{F}_{\text{BB}}^{\text{opt}}) = \underset{\mathbf{F}_{\text{BB}}, \mathbf{F}_{\text{RF}}}{\operatorname{argmin}} \left\|\mathbf{F}_{\text{opt}} - \mathbf{F}_{\text{RF}}\mathbf{F}_{\text{BB}}\right\|_{\text{F}}, \\ \text{s.t.} \quad \mathbf{F}_{\text{RF}} \in \mathcal{F}_{\text{RF}}, \\ \left\|\mathbf{F}_{\text{RF}}\mathbf{F}_{\text{BB}}\right\|_F^2 = N_s\end{aligned} \tag{1.7}$$

Since the feasible set $\mathcal{F}_{\mathcal{RF}}$ is non-convex, the task of finding the optimal matrices is both analytically and algorithmically intractable. The authors use the following observations to arrive upon the "Orthogonal Matching Pursuit Algorithm" to find the optimal RF and BB precoders.

1. The columns of the unitary matrix $\mathbf{V}$ form an orthonormal basis for the channel's row space.
2. The channel array response vectors $\mathbf{a_r}(\phi_{il}^r, \theta_{il}^r)$ and $\mathbf{a_t}(\phi_{il}^t, \theta_{il}^t)$ also form a spanning set for the channel's row space. Further, for $N_{cl}N_{ray} \leq N_t$, the array response vectors are independent and hence they form a basis for the channel's row space.
3. The columns of F_{opt} can be written as linear combinations of the array response vectors.
4. The array response vectors $\mathbf{a_t}(\phi_{il}^t, \theta_{il}^t)$ are constant magnitude and can be implemented at RF using the phase shifters. Thus, the design problem is to find the set of N_t^{RF} vectors to find the linear combination that minimizes $\left\|\mathbf{F}_{\text{opt}} - \mathbf{F}_{\text{RF}}\mathbf{F}_{\text{BB}}\right\|_{\text{F}}$.

This leads to the following equivalent problem:

$$\begin{aligned}\widetilde{\mathbf{F}}_{\text{BB}}^{\text{opt}} = \underset{\widetilde{\mathbf{F}}_{\text{BB}}}{\operatorname{argmin}} \left\|\mathbf{F}_{\text{opt}} - \mathbf{A}_{\text{t}}\widetilde{\mathbf{F}}_{\text{BB}}\right\|_{\text{F}}, \\ \text{s.t.} \quad \left\|\text{diag}(\widetilde{\mathbf{F}}_{\text{BB}}\widetilde{\mathbf{F}}_{\text{BB}}^{\text{H}})\right\|_0 = N_t^{\text{RF}}, \\ \left\|\mathbf{A}_{\text{t}}\widetilde{\mathbf{F}}_{\text{BB}}\right\|_F^2 = N_s\end{aligned} \tag{1.8}$$

where $\mathbf{A}_{\mathrm{t}}$ is the $N_t \times N_{cl} N_{ray}$ matrix of array response vectors and $\widetilde{\mathbf{F}}_{\mathrm{BB}}$ cannot have more than N_t^{RF} non-zero rows. Quoting the paper, "Essentially, we have reformulated the problem of jointly designing $\mathbf{F}_{\mathrm{RF}}$ and $\mathbf{F}_{\mathrm{BB}}$ into a sparsity constrained matrix reconstruction problem with one variable". The pseudo-code for the algorithm is as in figure 1.2.

Algorithm 1 Spatially Sparse Precoding via Orthogonal Matching Pursuit

Require: $\mathbf{F}_{\mathrm{opt}}$

$\mathbf{F}_{\mathrm{RF}} = \text{Empty Matrix}$

$\mathbf{F}_{\mathrm{res}} = \mathbf{F}_{\mathrm{opt}}$

for $i \leq N_{\mathrm{t}}^{\mathrm{RF}}$ **do**

$\quad \mathbf{\Psi} = \mathbf{A}_t^* \mathbf{F}_{\mathrm{res}}$

$\quad k = \arg\max_{\ell=1,\ \ldots,\ N_{\mathrm{cl}} N_{\mathrm{ray}}} (\mathbf{\Psi}\mathbf{\Psi}^*)_{\ell,\ell}$

$\quad \mathbf{F}_{\mathrm{RF}} = \left[\mathbf{F}_{\mathrm{RF}} | \mathbf{A}_t^{(k)}\right]$

$\quad \mathbf{F}_{\mathrm{BB}} = \left(\mathbf{F}_{\mathrm{RF}}^* \mathbf{F}_{\mathrm{RF}}\right)^{-1} \mathbf{F}_{\mathrm{RF}}^* \mathbf{F}_{\mathrm{opt}}$

$\quad \mathbf{F}_{\mathrm{res}} = \frac{\mathbf{F}_{\mathrm{opt}} - \mathbf{F}_{\mathrm{RF}} \mathbf{F}_{\mathrm{BB}}}{\|\mathbf{F}_{\mathrm{opt}} - \mathbf{F}_{\mathrm{RF}} \mathbf{F}_{\mathrm{BB}}\|_F}$

end for

$\mathbf{F}_{\mathrm{BB}} = \sqrt{N_{\mathrm{s}}} \frac{\mathbf{F}_{\mathrm{BB}}}{\|\mathbf{F}_{\mathrm{RF}} \mathbf{F}_{\mathrm{BB}}\|_F}$

return $\mathbf{F}_{\mathrm{RF}},\ \mathbf{F}_{\mathrm{BB}}$

Figure 1.2: Orthogonal Matching Pursuit algorithm (Ayach *et al.* (2014))

Algorithm 2 Spatially Sparse MMSE Combining via Orthogonal Matching Pursuit

Require: $\mathbf{W}_{\mathrm{MMSE}}$

$\mathbf{W}_{\mathrm{RF}} = \text{Empty Matrix}$

$\mathbf{W}_{\mathrm{res}} = \mathbf{W}_{\mathrm{MMSE}}$

for $i \leq N_{\mathrm{r}}^{\mathrm{RF}}$ **do**

$\quad \mathbf{\Psi} = \mathbf{A}_r^* \mathbb{E}\left[\mathbf{y}\mathbf{y}^*\right] \mathbf{W}_{\mathrm{res}}$

$\quad k = \arg\max_{\ell=1,\ \ldots,\ N_{\mathrm{cl}} N_{\mathrm{ray}}} (\mathbf{\Psi}\mathbf{\Psi}^*)_{\ell,\ell}$

$\quad \mathbf{W}_{\mathrm{RF}} = \left[\mathbf{W}_{\mathrm{RF}} | \mathbf{A}_r^{(k)}\right]$

$\quad \mathbf{W}_{\mathrm{BB}} = \left(\mathbf{W}_{\mathrm{RF}}^* \mathbb{E}\left[\mathbf{y}\mathbf{y}^*\right] \mathbf{W}_{\mathrm{RF}}\right)^{-1} \mathbf{W}_{\mathrm{RF}}^* \mathbb{E}\left[\mathbf{y}\mathbf{y}^*\right] \mathbf{W}_{\mathrm{MMSE}}$

$\quad \mathbf{W}_{\mathrm{res}} = \frac{\mathbf{W}_{\mathrm{MMSE}} - \mathbf{W}_{\mathrm{RF}} \mathbf{W}_{\mathrm{BB}}}{\|\mathbf{W}_{\mathrm{MMSE}} - \mathbf{W}_{\mathrm{RF}} \mathbf{W}_{\mathrm{BB}}\|_F}$

end for

return $\mathbf{W}_{\mathrm{RF}},\ \mathbf{W}_{\mathrm{BB}}$

Figure 1.3: Orthogonal Matching Pursuit algorithm for receiver processing (Ayach *et al.* (2014))

We use a similar algorithm for the design of receiver decoders, the algorithm for which is shown in figure 1.3. We move on to our simulation results to emulate the results obtained in the paper.

1.2.4 Simulation results

We use the same parameter values as used in the paper to compare the OMP algorithm with the optimal digital precoder (unconstrained precoding - signals are sent on the channel's dominant eigenvectors) and beam-steering (data streams are sent on the best performing paths and received along the best corresponding receive paths). The inter-antenna-element spacing is taken to be half-wavelength. The results obtained by us are shown in figures 1.4 and 1.5 along with the parameter values for the same.

We obtain similar spectral efficiency values for the optimal digital precoder and the OMP algorithm but see some difference for the beam-steering values. Nevertheless, we see similar trends for both the systems with OMP outperforming beam steering (more significantly in our simulations).

1.3 Alternating Minimization

In this section, we look at the ideas and algorithms proposed in the paper by Yu *et al.* (2016). The authors propose two algorithms for the Fully Connected structure seen in figure 1.1 and an algorithm for a partially connected structure shown in figure 1.6.

1.3.1 Algorithms and Simulation Results

We will briefly look at the MO-Altmin and PE-Altmin algorithms proposed for the fully connected structure. The alternating minimization idea is to design the digital precoder $\mathbf{F}_{\text{BB}}$ for a fixed analog precoder $\mathbf{F}_{\text{RF}}$. This leads to the optimization problem

$$\underset{\mathbf{F}_{\text{BB}}}{\text{minimize}} \left\|\mathbf{F}_{\text{opt}} - \mathbf{F}_{\text{RF}}\mathbf{F}_{\text{BB}}\right\|_{\text{F}} \tag{1.9}$$

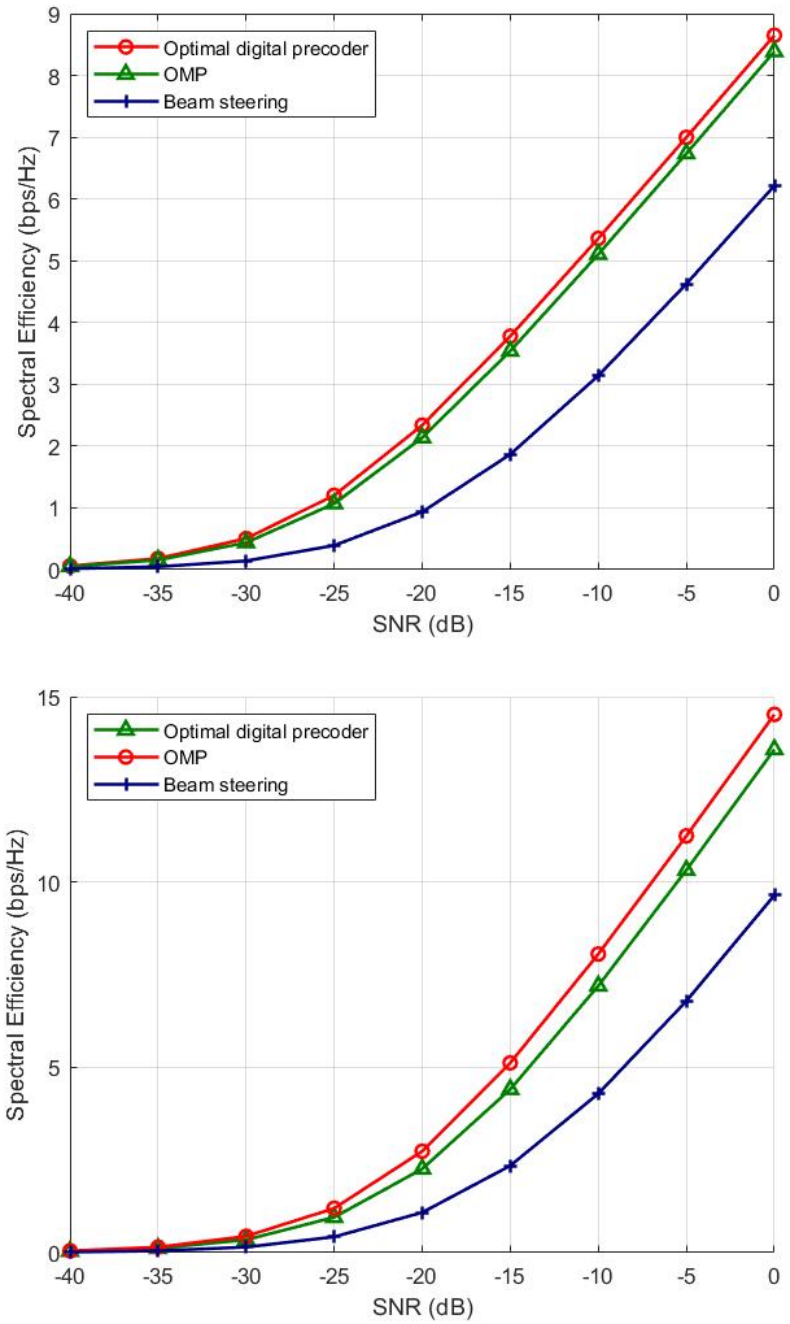

Figure 1.4: OMP - Spectral efficiency achieved for a 64 × 16 mmWave system with $N_{cl} = 8$, $N_{ray} = 10$, an angular spread of 7.5° and 4 RF chains. The plot on top is for $N_s = 1$ while that on bottom is for $N_s = 2$. The plots are shown separately for convenience.

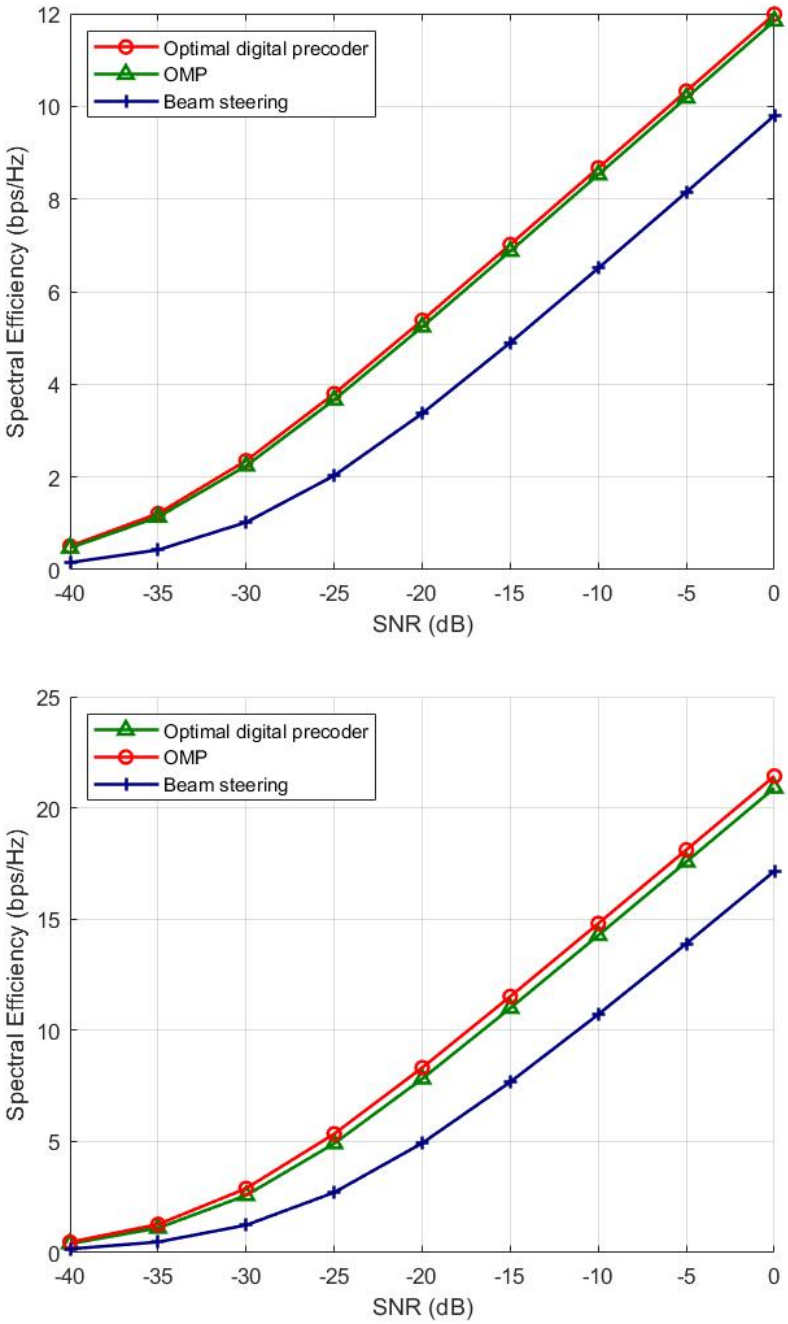

Figure 1.5: OMP - Spectral efficiency achieved for a 256 × 64 mmWave system with $N_{cl} = 8$, $N_{ray} = 10$, an angular spread of 7.5° and 6 RF chains. The plot on top is for $N_s = 1$ while that on bottom is for $N_s = 2$. The plots are shown separately for convenience.

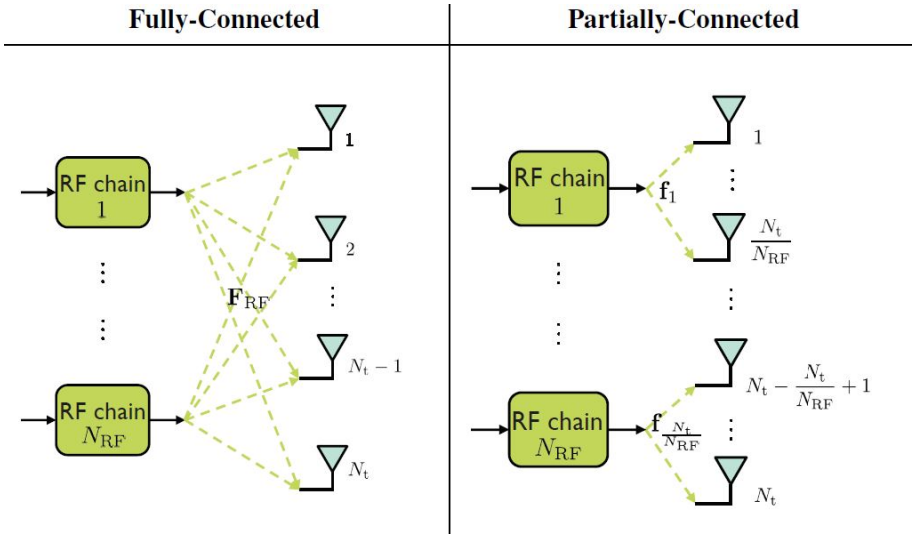

Figure 1.6: Fully and partially connected mapping structure for hybrid precoding (Zhang *et al.* (2020)).

which has a solution given by the least-squares solution given by

$$\mathbf{F}_{\text{BB}} = \mathbf{F}_{\text{RF}}^{\dagger}\mathbf{F}_{\text{opt}} \tag{1.10}$$

In MO-AltMin, for the next part of the algorithm (finding optimal $\mathbf{F}_{\text{RF}}$ for a given $\mathbf{F}_{\text{BB}}$, the authors consider an effective manifold optimization algorithm to find a near-optimal solution. However, the number of constraints for the MO-AltMin algorithm can be very high which might restrict its practical implementation. Thus the authors propose a low complexity algorithm which extracts the phases of the analog precoder from those of the digital precoder and the optimal precoder.

The idea behing the PE-AltMin algorithm is that the columns of $\mathbf{F}_{\text{opt}}$ are orthogonal and hence we impose a similar constraint on the columns of $\mathbf{F}_{\text{BB}}$, i.e.

$$\mathbf{F}_{\text{BB}} = \alpha\mathbf{F}_{\text{DD}} \tag{1.11}$$

where $\mathbf{F}_{\text{DD}}$ is a unitary matrix. The authors show that the optimization problem is

modified to

$$\underset{\mathbf{F}_{\text{DD}},\mathbf{F}_{\text{RF}}}{\text{minimize}} \left\|\mathbf{F}_{\text{opt}}\mathbf{F}_{\text{DD}}^{\text{H}} - \mathbf{F}_{\text{RF}}\right\|_{\text{F}}^{\mathbf{2}}, \tag{1.12}$$

$$\text{subject to} \quad |(\mathbf{F}_{\text{RF}})_{i,j}| = 1, \forall i, j$$

$$\mathbf{F}_{\text{DD}}^{H}\mathbf{F}_{\text{DD}} = I_{N_s}$$

the solution for which during alternating minimization is given by

$$\arg(\mathbf{F}_{\text{RF}}) = \arg(\mathbf{F}_{\text{opt}}\mathbf{F}_{\text{DD}}^{\text{H}}) \tag{1.13}$$

where $\arg$ extracts the phase elementwise for the matrix. In the next step of alternating minimization, $\mathbf{F}_{\text{DD}}$ is found as

$$\mathbf{F}_{\text{DD}} = \mathbf{V_1}\mathbf{U}^{H} \tag{1.14}$$

where the $\text{SVD}(\mathbf{F}_{\text{opt}}^{H}\mathbf{F}_{\text{RF}}) = \mathbf{U}\mathbf{\Sigma}\mathbf{V}^{H}$ and V_1 denotes the first N_s columns of V. The PE-AltMin algorithm is shown in figure 1.7.

PE-AltMin Algorithm: A Low-Complexity Algorithm for the Fully-connected Structure

Input: $\mathbf{F}_{\text{opt}}$

1: Construct $\mathbf{F}_{\text{RF}}^{(0)}$ with random phases and set $k = 0$;
2: **repeat**
3: Fix $\mathbf{F}_{\text{RF}}^{(k)}$, compute the SVD: $\mathbf{F}_{\text{opt}}^{H}\mathbf{F}_{\text{RF}}^{(k)}=\mathbf{U}^{(k)}\mathbf{S}^{(k)}{\mathbf{V}_1^{(k)}}^{H}$;
4: $\mathbf{F}_{\text{DD}}^{(k)} = \mathbf{V}_1^{(k)}{\mathbf{U}^{(k)}}^{H}$;
5: Fix $\mathbf{F}_{\text{DD}}^{(k)}$, and $\arg\left\{\mathbf{F}_{\text{RF}}^{(k+1)}\right\} = \arg\left(\mathbf{F}_{\text{opt}}{\mathbf{F}_{\text{DD}}^{(k)}}^{H}\right)$;
6: $k \leftarrow k + 1$;
7: **until** a stopping criterion triggers;
8: For the digital precoder at the transmit end, normalize $\widehat{\mathbf{F}}_{\text{BB}} = \frac{\sqrt{N_s}}{\|\mathbf{F}_{\text{RF}}\mathbf{F}_{\text{DD}}\|_F}\mathbf{F}_{\text{DD}}$.

Figure 1.7: Phase Extraction (PE) - AltMin Algorithm (Yu *et al.* (2016))

For the partially connected structure, the authors use a Semidefinite Relaxation based AltMin algorithm to get an approximate solution to the problem. The output

of each RF chain is connected to only N_t/N_t^{RF} antennas which significantly reduces the hardware complexity. The authors also show that the proposed Alternating Minimization algorithms can also be applied for MIMO-OFDM systems.

We will look at the plots comparing these algorithms to OMP (as a benchmark for the fully connected structure) and Successive Interference Cancellation (as a benchmark for the partially connected structure) in figures 1.8 and . The code for most of these algorithms is taken from Xianghao (2016).

Our setup for the simulations is similar to the one used for OMP in subsection 1.2.4 with the parameter values as follows: we use $N_t = 144$, $N_r = 36$, $N_{cl} = 5$ and $N_{ray} = 10$. The other parameter values used are mentioned in the captions.

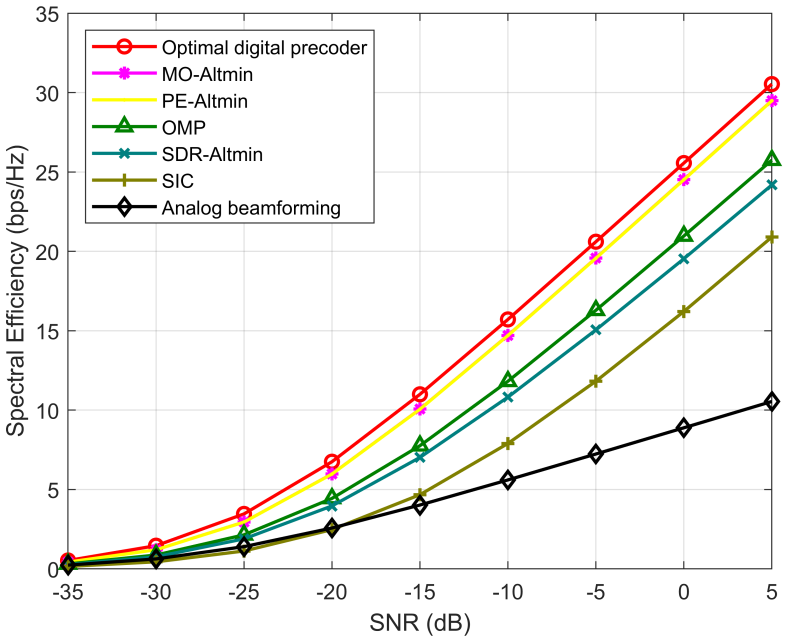

Figure 1.8: AltMin - Spectral Efficiency Comparison - AltMin algorithms, $N_s = N_t^{RF} = N_r^{RF} = 3$

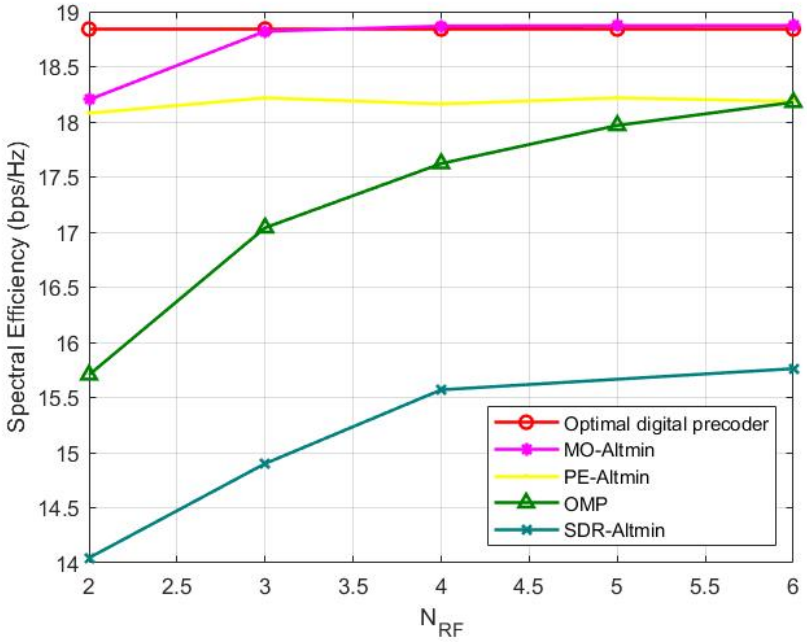

Figure 1.9: AltMin - Spectral Efficiency vs N_{RF}, $N_s = 2$, $N_t^{RF} = N_r^{RF} = N_{RF}$

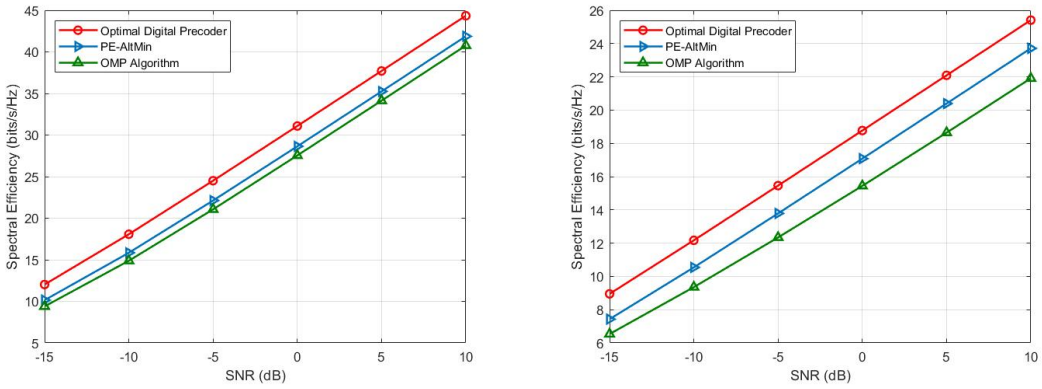

Figure 1.10: AltMin - Spectral Efficiency in MIMO-OFDM systems - a) $N_s = 4$, $N_{RF} = 5$, b) $N_s = N_{RF} = 2$

1.4 Double Phase Shifter and Fixed Phase Shifter

In Zhang *et al.* (2020) and Yu *et al.* (2018), the authors propose two new hardware implementations for the hybrid precoding problem for the fully connected structure and partially connected structure respectively.

1.4.1 Multi-User MIMO setting

We briefly look at the Multi-User MIMO setting considered in Zhang *et al.* (2020) (Figure 1.11). The model considers K users, each with N_r^{RF} receive antennas and a total of F subcarriers. The optimization problem for this setting is as below:

$$\begin{aligned} \underset{\mathbf{F}_{\text{BB}},\mathbf{F}_{\text{RF}}}{\text{minimize}} \; & \|\mathbf{F}_{\text{opt}} - \mathbf{F}_{\text{RF}}\mathbf{F}_{\text{BB}}\|_{\text{F}}, \\ \text{s.t.} \quad & \mathbf{F}_{\text{RF}} \in \mathcal{F}_{\text{RF}}, \\ & \|\mathbf{F}_{\text{RF}}\mathbf{F}_{\text{BB}}\|_F^2 \leq KN_sF \end{aligned} \tag{1.15}$$

where the combined fully digital precoder $\mathbf{F}_{\text{opt}}$ is the concatenation of the individual optimal precoders $\mathbf{F}_{\text{opt}} = [\mathbf{F}_{\text{opt}_{\mathbf{1},\mathbf{1}}}, ..., \mathbf{F}_{\text{opt}_{\mathbf{k},\mathbf{f}}}, ..., \mathbf{F}_{\text{opt}_{\mathbf{K},\mathbf{F}}}]$ and similarly for $\mathbf{F}_{\text{BB}}$.

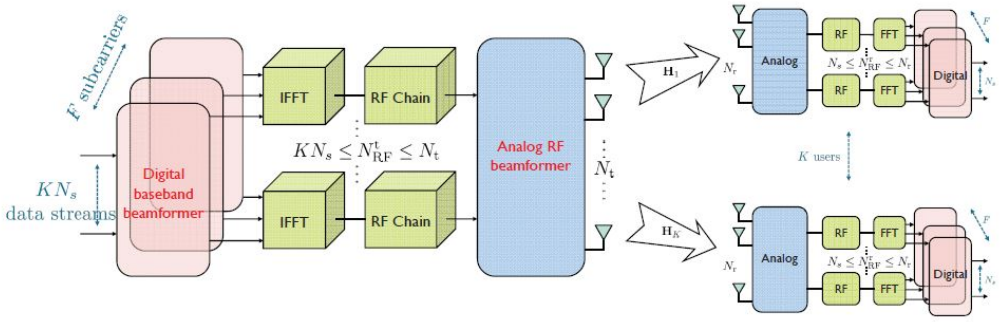

Figure 1.11: MU-MIMO system with Hybrid precoding Zhang *et al.* (2020)

1.4.2 Double Phase Shifter (DPS) implementation

The authors state that the main problem for the Single Phase Shifter designs seen so far is the unit modulus constraint on $\mathbf{F}_{\text{RF}}$. To overcome this, the authors consider the Double Phase Shifter (DPS) approach where we have two sets of phase shifters as seen in figure 1.12. This increases the hardware complexity but decreases the algorithmic complexity - there are efficient algorithms for the modified optimization problem as seen in Yu *et al.* (2019). The difference in spectral efficiency as compared to the single phase shifter designs is further amplified in the multi-user scenario as seen in figure 1.13 taken from Yu *et al.* (2019).

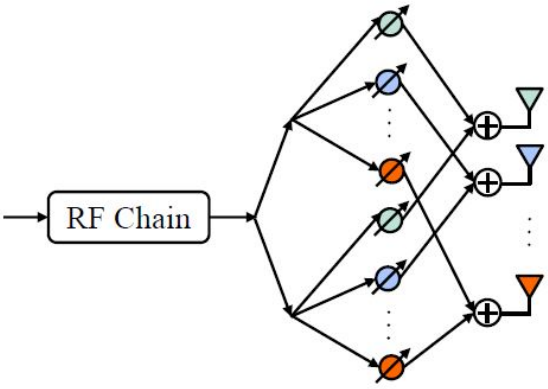

Figure 1.12: DPS implementation for Hybrid beamforming (Zhang *et al.*, 2020)

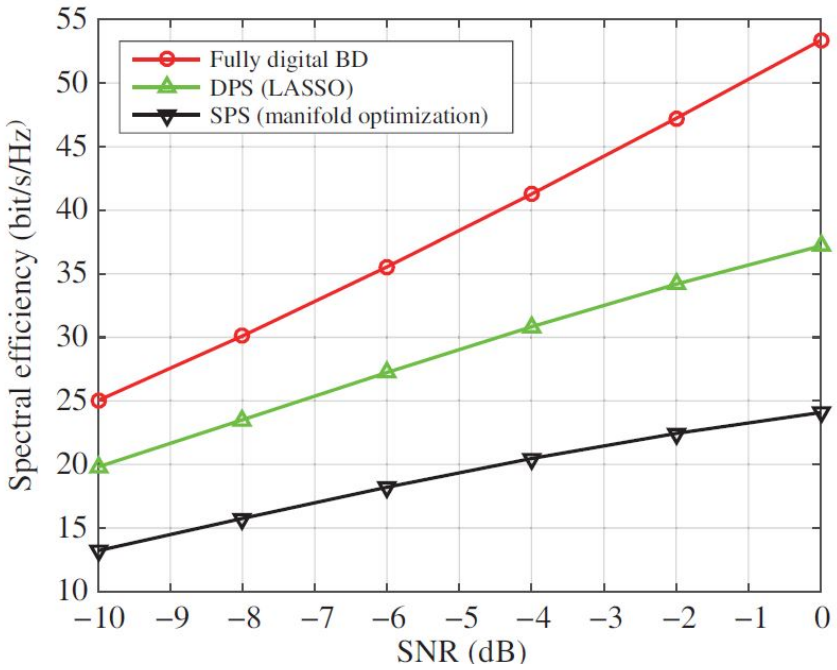

Figure 1.13: DPS - Spectral Efficiency for MU-MIMO (Zhang *et al.*, 2020) with $N_t = 64, N_r = 9, K = 5, N_s = 2, N_t^{RF} = KN_r^{RF} = KN_s$

The authors show that the DPS fully-connected mapping optimization problem is that of a low-rank matrix approximation reconstructing $\mathbf{F}_{\text{RF}}\mathbf{F}_{\text{BB}}$ using the first N_t^{RF} columns of its SVD matrices. This also leads to another SPS implementation based on extracting the phase from the DPS matrices. The performance of these 2 implementations is shown in figures 1.14 and 1.15.

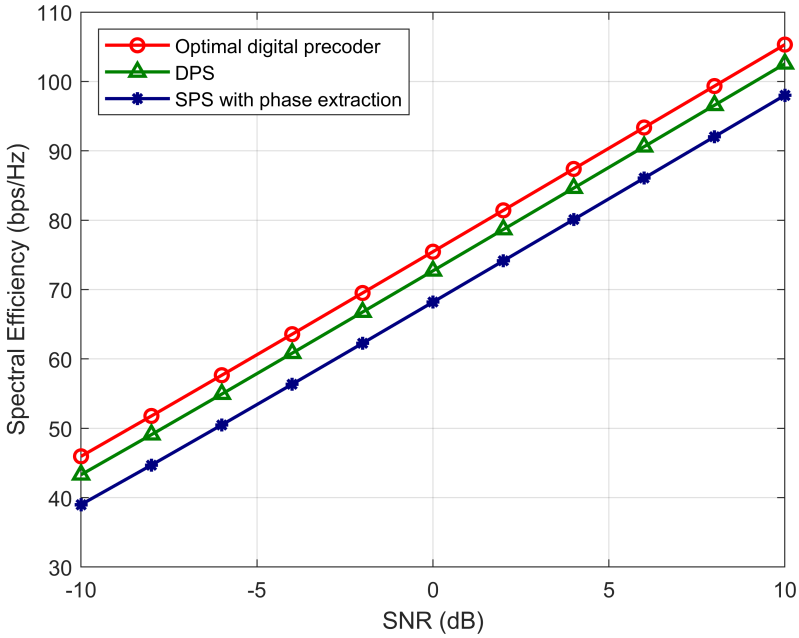

Figure 1.14: DPS - Spectral Efficiency for MU-MIMO with $N_t = 256, N_r = 16, K = 3, N_s = 3, N_t^{RF} = N_r^{RF} = 6$

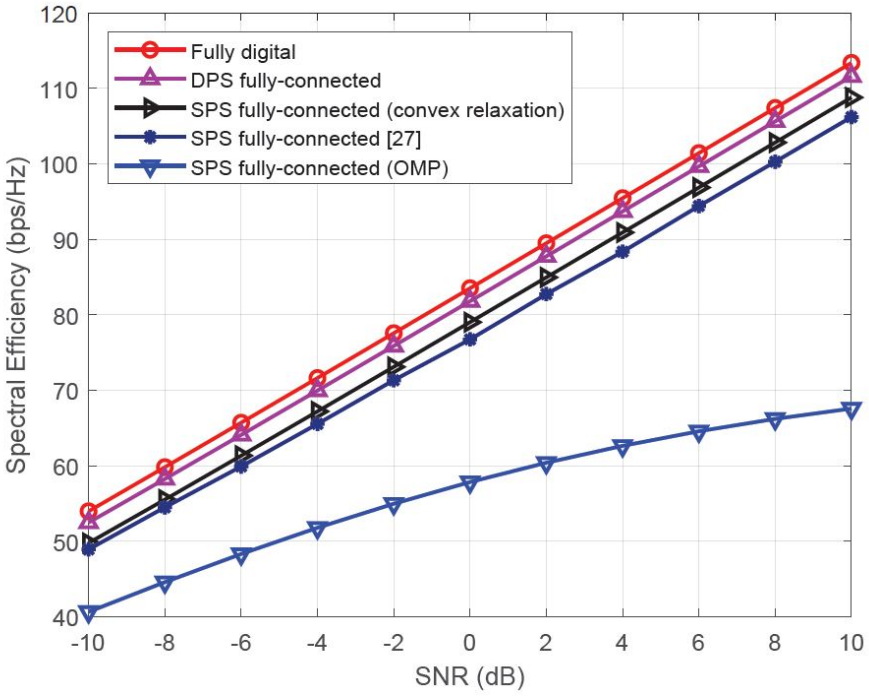

Figure 1.15: DPS - Spectral Efficiency for MU-MIMO (Plot from Zhang *et al.* (2020)) with $N_t = 256, N_r = 16, K = 3, N_s = 3$

1.4.3 Fixed Phase Shifter (FPS) implementation

The authors proposed the FPS implementation in Yu *et al.* (2018) to overcome the hardware complexity of the DPS implementation while using the benefit of passing the output of an RF chain through multiple phase shifters. The algorithm and idea detailed in Yu *et al.* (2018) is briefly explain here.

Instead of having a single or double phase shifter from each RF chain to antenna element, the FPS implementation uses a fixed number of fixed phase multichannel phase shifters (phase shifters that can simultaneously process inputs from N_t^{RF} RF chains) and an adaptive switch network to connect the outputs of the phase shifters to the antenna elements. The authors show that the FPS-fully connected implementation outperforms the PE-AltMin and OMP implementations as can be seen from figures 1.16 and 1.17.

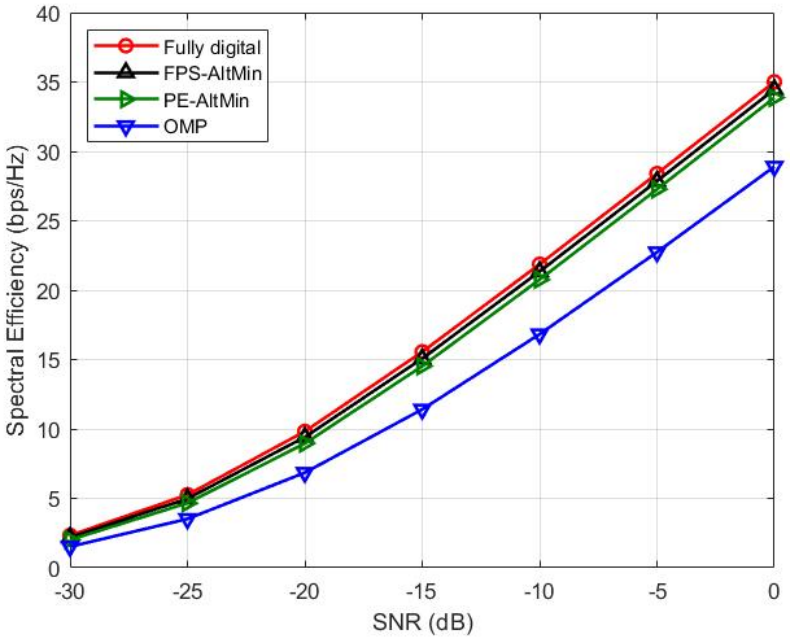

Figure 1.16: FPS - Spectral Efficiency for SU-MIMO with $N_t = 144$, $N_r = 16$, $N_t^{RF} = N_r^{RF} = N_s = 4$ and $N_c = 30$

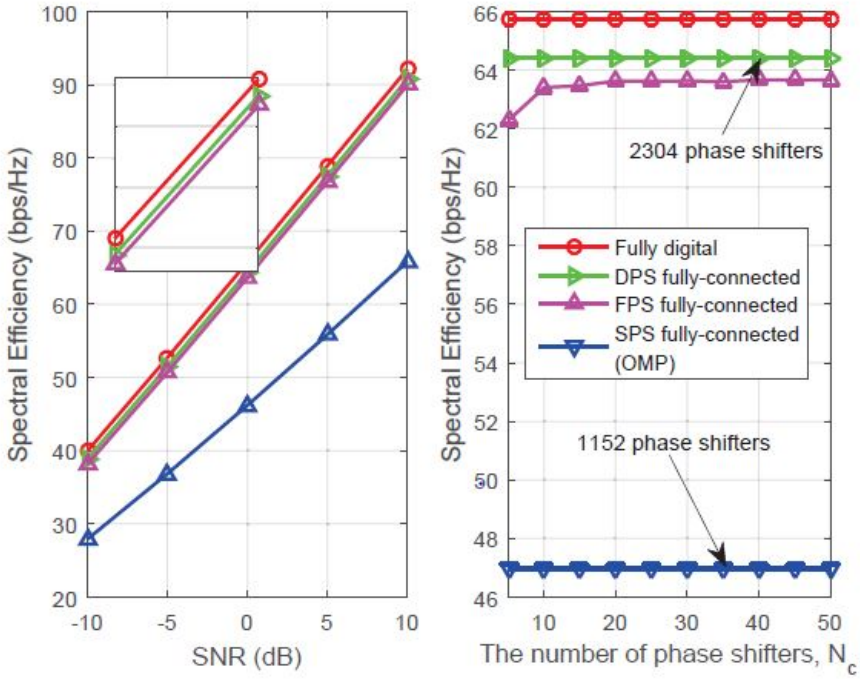

Figure 1.17: FPS - Spectral Efficiency comparison from Zhang *et al.* (2020)

CHAPTER 2

Channel Estimation and Hybrid Precoding

2.1 Introduction

In this chapter, we briefly look at the channel estimation algorithm proposed in Alkhateeb *et al.* (2014) and simulate some of the algorithms seen in the previous chapter in the case of channel estimated with the channel estimation algorithm.

The system model we consider in this chapter is similar to that in Hybrid precoding except for some changes outlined in this paragraph. Instead of Uniform Planar Array (UPA), we assume a Uniform Linear Array structure. The array response vectors can be written as

$$\mathbf{a}(\phi_l) = \frac{1}{\sqrt{N}}\left[1, e^{j\frac{2\pi}{\lambda}dsin(\phi_l)}, ..., e^{j\frac{2\pi}{\lambda}d(N-1)sin(\phi_l)}\right]^T \tag{2.1}$$

The channel $\mathbf{H}$ can be expressed as

$$\mathbf{H} = \gamma \sum_{l=1}^{L} \alpha_l \mathbf{a_r}(\phi_l^r)\mathbf{a_t}(\phi_l^t)^H \tag{2.2}$$

where L is the total number of scattering paths.

The channel estimation algorithm needs to estimate the Angle of Departure (AoD), Angle of Arrival (AoA) and magnitude for each path to get an estimate of the channel. The idea behind the proposed channel estimation algorithm is briefly explained here. We assume that the resolution for AoA and AoD is N, i.e., we assume that the AoAs and AoDs are taken from a discrete set of N points $\{0, \frac{2\pi}{N}, ..., \frac{2\pi(N-1)}{N}\}$. Estimating the AoA and AoD as the angles maximizing the received signal power (the naive approach) would require N^2 measurements by transmitting using all N transmit channel vectors and receiving every transmit channel vector with every receive channel vector. The authors have shown that the required number of measurements L is significantly lesser than N^2 and have proposed an algorithm using binary search, that makes $K^2 log_K(N)$ measurements to estimate the AoA and AoD for a parameter K.

2.2 Multi-resolution based hierarchical codebook

The authors propose a hybrid analog-digital codebook $\mathcal{F}$ consisting of $S = log_K(N)$ levels with each level containing beamforming vectors with a certain beamwidth to be used in the corresponding training stage of the channel estimation algorithm. At each level, the AoD range under consideration is divided into K subranges and so on. The K beamforming vectors are designed so as to have non-zero projection on the corresponding channel response vector and zero projection on the other vectors.

The authors show that the approximate solution for this problem is given by $\mathbf{F}_{s,k} = (\mathbf{A}_{t,D}\mathbf{A}_{t,D}^H)^\dagger \mathbf{A}_{t,D}\mathbf{G}_{s,k}$ where $\mathbf{A}_{t,D}$ is a dictionary matrix of channel response vectors for the N discrete AoD values and $\mathbf{G}_{s,k}$ is an $N \times K$ matrix with each column containing 1's in the locations belonging to the corresponding AoD range. The algorithm for the design of the codebook, which is similar to the OMP design, is shown in figure 2.1 taken from the paper.

Algorithm 1 Hybrid Analog-Digital Training Precoders Design

$\mathcal{R} = \phi$

$\mathbf{f}_{\text{res}} = (\mathbf{A}_{\text{BS,D}}\mathbf{A}_{\text{BS,D}}^H)^{-1}\mathbf{A}_{\text{BS,D}} \left[\mathbf{G}_{(s,k)}\right]_{:,m}$

$\mathbf{f}^\star = (\mathbf{A}_{\text{BS,D}}\mathbf{A}_{\text{BS,D}}^H)^{-1}\mathbf{A}_{\text{BS,D}} \left[\mathbf{G}_{(s,k)}\right]_{:,m}$

for $i \leq N_{\text{RF}}$ **do**

$\mathbf{\Phi} = \mathbf{f}_{\text{res}}^H \mathbf{A}_{\text{can}}$

$n = \arg\max_{n=1,2,..N_{\text{can}}} \left[\mathbf{\Phi}^H \mathbf{\Phi}\right]_{i,i}$

$\mathcal{R} = \mathcal{R} \cup n$

$\mathbf{F}_{\text{RF},(s,k)} = [\mathbf{A}_{\text{can}}]_{:,\mathcal{R}}$

$\left[\mathbf{F}_{\text{BB},(s,k)}\right]_{:,m} = \left(\mathbf{F}_{\text{RF},(s,k)}{}^H \mathbf{F}_{\text{RF},(s,k)}\right)^{-1} \mathbf{F}_{\text{RF},(s,k)}^H \mathbf{f}^\star$

$\mathbf{f}_{\text{res}} = \frac{\mathbf{f}_{\text{res}} - \mathbf{F}_{\text{RF},(s,k)}[\mathbf{F}_{\text{BB},(s,k)}]_{:,m}}{\|\mathbf{f}_{\text{res}} - \mathbf{F}_{\text{RF},(s,k)}[\mathbf{F}_{\text{BB},(s,k)}]_{:,m}\|_F}$

$C_s = \sqrt{\frac{1}{\|\mathbf{F}_{\text{RF},(s,k)}[\mathbf{F}_{\text{BB},(s,k)}]_{:,m}\|_F}}$

$\left[\mathbf{F}_{\text{BB},(s,k)}\right]_{:,m} = C_s \left[\mathbf{F}_{\text{BB},(s,k)}\right]_{:,m}$

Figure 2.1: Channel Estimation - Hierarchical Codebook Design (Alkhateeb *et al.*, 2014).

2.3 Adaptive Estimation Algorithm

We divide the AoD and AoA range into K subranges each and find the respective subrange corresponding to the maximum power and consider these ranges in the next iteration of the algorithm. The algorithm for the single path channel with the discussed hierarchical codebook is shown in figure 2.2.

Algorithm 2 Adaptive Estimation Algorithm for Single-Path MmWave Channels

Input: BS and MS know N, K, and have $\mathcal{F}, \mathcal{W}$.

Initialization: $k_1^{\mathrm{BS}} = 1, k_1^{\mathrm{MS}} = 1$ // Initialize the subsets to be used of codebooks $\mathcal{F}, \mathcal{W}$

$\mathrm{S} = \log_K N$ // The number of adaptive stages

for $s \leq \mathrm{S}$ **do**

  for $m_{\mathrm{BS}} \leq K$ **do**

    BS transmits a training symbol using $\left[\mathbf{F}_{(s,k_s^{\mathrm{BS}})}\right]_{:,m_{\mathrm{BS}}}$

    for $m_{\mathrm{MS}} \leq K$ **do**

      MS makes a measurement using $\left[\mathbf{W}_{(s,k_s^{\mathrm{MS}})}\right]_{:,m_{\mathrm{MS}}}$

    After MS measurements: $\mathbf{y}_{m_{\mathrm{BS}}} = \sqrt{P_s}\left[\mathbf{W}_{(s,k_s^{\mathrm{MS}})}\right]\mathbf{H}\left[\mathbf{F}_{(s,k_s^{\mathrm{BS}})}\right]_{:,m_{\mathrm{BS}}} + \mathbf{n}_{m_{\mathrm{BS}}}$

  $\mathbf{Y}_{(s)} = [\mathbf{y}_1, \mathbf{y}_2, ..., \mathbf{y}_K]$

  $(m_{\mathrm{BS}}^{\star}, m_{\mathrm{MS}}^{\star}) = \arg\max_{\forall m_{\mathrm{BS}}, m_{\mathrm{MS}}=1,2,...,K}\left[\mathbf{Y}_{(s)} \odot \mathbf{Y}_{(s)}^{*}\right]_{m_{\mathrm{MS}}, m_{\mathrm{BS}}}$

  $k_{s+1}^{\mathrm{BS}} = K(m_{\mathrm{BS}}^{\star} - 1) + 1, k_{s+1}^{\mathrm{MS}} = K(m_{\mathrm{MS}}^{\star} - 1) + 1$

$\hat{\phi} = \bar{\phi}_{k_{\mathrm{S}+1}^{\mathrm{BS}}}, \hat{\theta} = \bar{\theta}_{k_{\mathrm{S}+1}^{\mathrm{MS}}}$

$\hat{\alpha} = \sqrt{\frac{\rho}{P_{(\mathrm{S})}G_{(\mathrm{S})}}}\left[\mathbf{Y}_{(\mathrm{S})}\right]_{m_{\mathrm{MS}}^{\star}, m_{\mathrm{BS}}^{\star}}$

Figure 2.2: Channel Estimation algorithm - Single path channel (Alkhateeb *et al.*, 2014).

For the multi-path scenario, we need to estimate L_d AoDs, AoAs and path gains. For this, the hierarchical codebooks are modified such that at each stage, we consider $K \times L_d$ subranges; L_d of these are chosen for the next stage with these subranges divided into K subranges each. The algorithm is shown in figure 2.3.

Algorithm 3 Adaptive Estimation Algorithm for Multi-Path MmWave Channels

Input: BS and MS know N, K, L_d, and have $\mathcal{F}, \mathcal{W}$

Initialization: $\mathbf{T}^{\mathrm{BS}}_{(1,1)} = \{1, ..., 1\}, \mathbf{T}^{\mathrm{MS}}_{(1,1)} = \{1, ..., 1\}, \mathrm{S} = \log_K (N/L_d)$

for $\ell \leq L_d$ **do**

  for $s \leq \mathrm{S}$ **do**

    for $m_{\mathrm{BS}} \leq KL_d$ **do**

      BS transmits a training symbol using $\left[\mathbf{F}_{(s,\mathbf{T}^{\mathrm{BS}}_{(\ell,s)})}\right]_{:,m_{\mathrm{BS}}}$

      for $m_{\mathrm{MS}} \leq KL_d$ **do**

        MS makes a measurement using $\left[\mathbf{W}_{(s,\mathbf{T}^{\mathrm{BS}}_{(\ell,s)})}\right]_{:,m_{\mathrm{MS}}}$

        After MS measurements: $\mathrm{y}_{m_{\mathrm{BS}}} = \sqrt{P_s}\left[\mathbf{W}_{(s,\mathbf{T}^{\mathrm{MS}}_{(\ell,s)})}\right]\mathbf{H}\left[\mathbf{F}_{(s,\mathbf{T}^{\mathrm{BS}}_{(\ell,s)})}\right]_{:,m_{\mathrm{BS}}} + \mathbf{n}_{m_{\mathrm{BS}}}$

    $\mathrm{y}_{(s)} = [\mathrm{y}_1^T, \mathrm{y}_2^T, ..., \mathrm{y}_K^T]^T$

    for $p = 1 \leq \ell - 1$ **do** Project out the contributions of the previously estimated paths

      $\mathbf{g} = \mathbf{F}^T_{(s,\mathbf{T}^{\mathrm{BS}}_{(p,s)})}[\mathbf{A}_{\mathrm{BS,D}}]^*_{:,\mathbf{T}^{\mathrm{BS}}_{(p,s)}(1)} \otimes \mathbf{W}^H_{(s,\mathbf{T}^{\mathrm{MS}}_{(p,s)})}[\mathbf{A}_{\mathrm{MS,D}}]_{:,\mathbf{T}^{\mathrm{MS}}_{(p,s)}(1)}$

      $\mathrm{y}_{(s)} = \mathrm{y}_{(s)} - \mathrm{y}^H_{(s)}\mathbf{g}\left(\mathbf{g}^H\mathbf{g}\right)\mathbf{g}$

    $\mathbf{Y} = \mathrm{matix}(\mathrm{y}_{(s)})$ Return $\mathrm{y}_{(s)}$ to the matrix form

    $(m^\star_{\mathrm{BS}}, m^\star_{\mathrm{MS}}) = \arg\max_{\forall m_{\mathrm{BS}}, m_{\mathrm{MS}}=1,2,...,K}[\mathbf{Y} \odot \mathbf{Y}^*]_{m_{\mathrm{MS}},m_{\mathrm{BS}}}$

    $\mathbf{T}^{\mathrm{BS}}_{(\ell,s+1)}(1) = K(m^\star_{\mathrm{BS}} - 1) + 1, \mathbf{T}^{\mathrm{MS}}_{(\ell,s+1)}(1) = K(m^\star_{\mathrm{MS}} - 1) + 1$

    for $p = 1 \leq \ell - 1$ **do**

      $\mathbf{T}^{\mathrm{BS}}_{(\ell,s+1)}(p) = \mathbf{T}^{\mathrm{BS}}_{(p,s+1)}(1), \mathbf{T}^{\mathrm{MS}}_{(\ell,s+1)}(p) = \mathbf{T}^{\mathrm{MS}}_{(p,s+1)}(1)$

  $\hat{\phi}_\ell = \bar{\phi}_{\mathbf{T}^{\mathrm{BS}}_{(\ell,\mathrm{S}+1)}(1)}, \hat{\theta}_\ell = \bar{\theta}_{\mathbf{T}^{\mathrm{MS}}_{(\ell,\mathrm{S}+1)}(1)}$

  $\mathbf{g} = \mathbf{F}^T_{(\mathrm{S},\mathbf{T}^{\mathrm{BS}}_{(\ell,\mathrm{S})})}\left[\mathbf{A}^*_{\mathrm{BS,D}}\right]_{:,\mathbf{T}^{\mathrm{BS}}_{(\ell,\mathrm{S}+1)}(1)} \otimes \mathbf{W}^H_{(\mathrm{S},\mathbf{T}^{\mathrm{MS}}_{(\ell,\mathrm{S})})}[\mathbf{A}_{\mathrm{MS,D}}]_{:,\mathbf{T}^{\mathrm{MS}}_{(\ell,\mathrm{S}+1)}(1)}$

  $\hat{\alpha}_\ell = \sqrt{\frac{\rho}{P_{(\mathrm{S})}G_{(\mathrm{S})}}}\frac{\mathrm{y}^H_{(\mathrm{S})}\mathbf{g}}{\mathbf{g}^H\mathbf{g}}$

Figure 2.3: Channel Estimation algorithm - Multi-path channel (Alkhateeb *et al.*, 2014)

.

Figure 2.6 shows the spectral efficiency comparison shown in Alkhateeb *et al.* (2014) comparing the algorithm with the computationally and time intensive exhaustive search for $N_t = 64, N_r = 32, L = 3$. Figures 2.4 and 2.5 compare PE-AltMin, FPS-AltMin and OMP for the single path case for $L = 1$ and $L = 3$ and we observe that the general trends seen in the perfect CSI scenario translate the channel estimation case as well. Note that for the single stream case ($L = 1$), there is no difference in performance of the different hybrid beamforming algorithms under consideration.

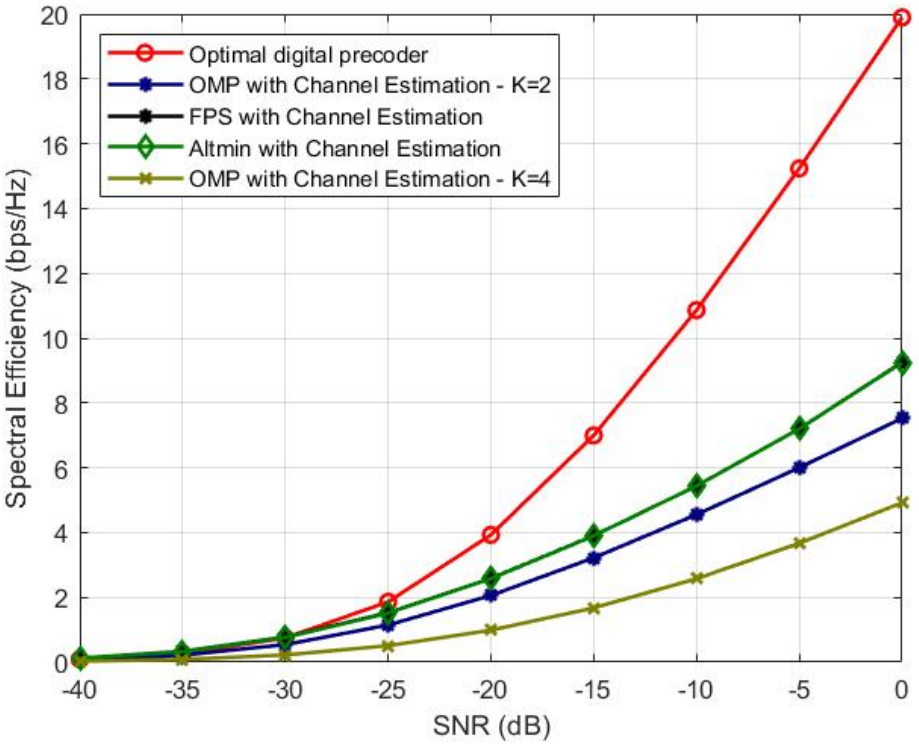

Figure 2.4: CE - Spectral Efficiency comparison for $L = 3$, $L_d = 1$

.

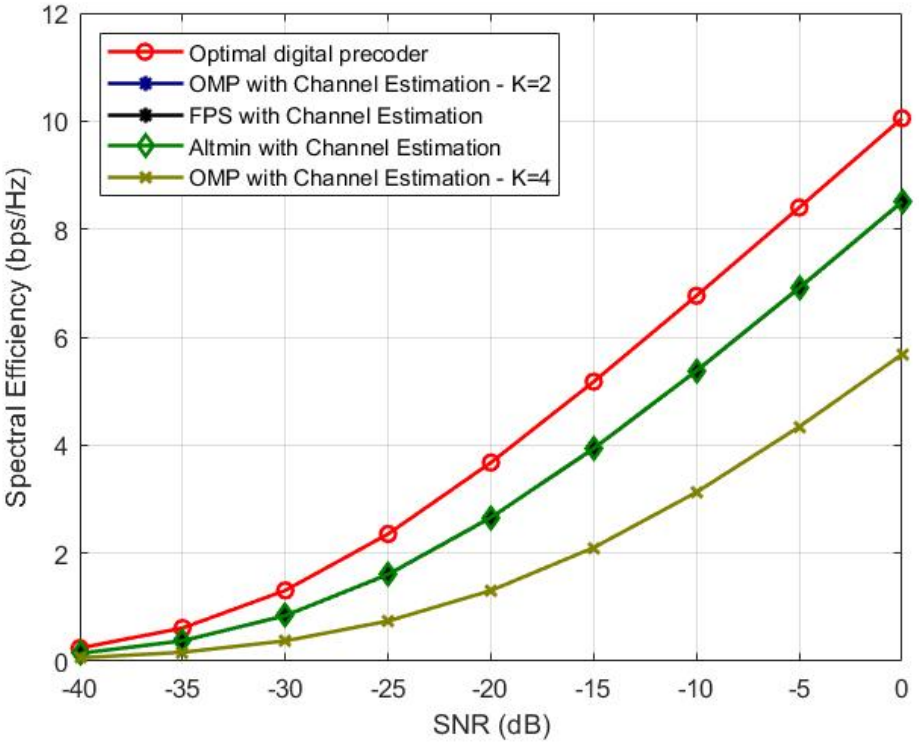

Figure 2.5: CE - Spectral Efficiency comparison for $L = 1$, $L_d = 1$

.

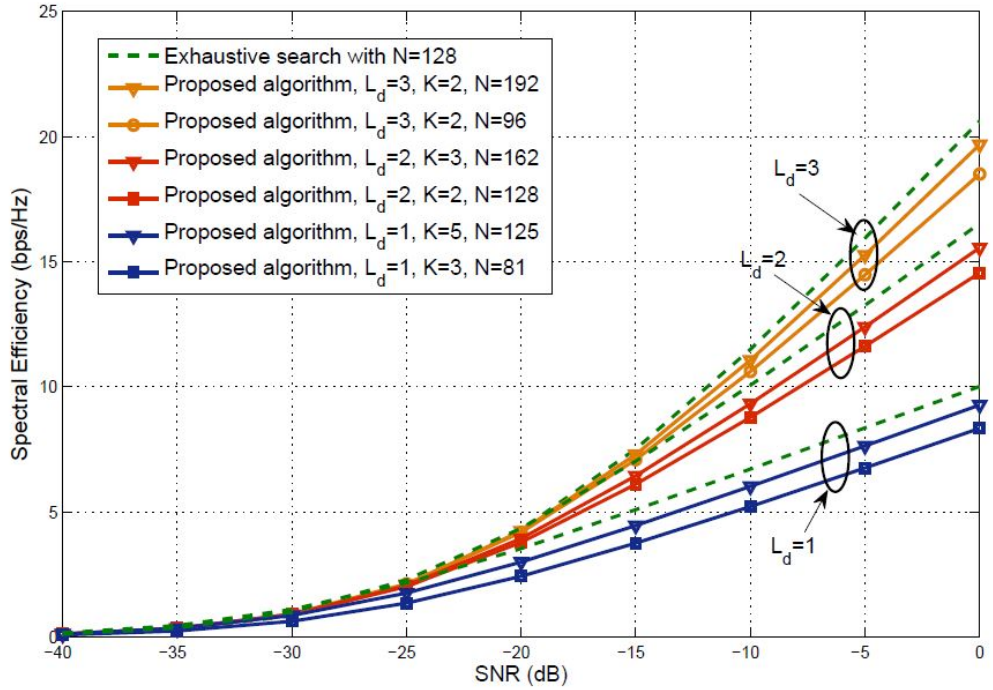

Figure 2.6: CE - Spectral Efficiency comparison for different L_d (Alkhateeb *et al.*, 2014)

.

CHAPTER 3

Summary

Through the course of this project, we have studied the different hybrid beamforming algorithms, namely the Orthogonal Matching Pursuit algorithm, the Alternating Minimization algorithms (Manifold Optimiziation-AltMin and Phase Extraction-AltMin) and the Double Phase Shifter and Fixed Phase Shifter hardware implementations and the corresponding algorithms and performed simulations wherever possible to replicate the results shown in the papers. We then looked at the Channel Estimation approach for hybrid beamforming and looked at the multi-resolution codebook and the Adaptive Estimation algorithm for channel estimation and compared some of the hybrid beamforming algorithms under the condition of imperfect CSI and perform simulations for the same.

REFERENCES

1. **Alkhateeb, A.**, **O. El Ayach**, **G. Leus**, and **R. W. Heath** (2014). Channel estimation and hybrid precoding for millimeter wave cellular systems. *IEEE Journal of Selected Topics in Signal Processing*, **8**(5), 831–846.

2. **Ayach, O. E.**, **S. Rajagopal**, **S. Abu-Surra**, **Z. Pi**, and **R. W. Heath** (2014). Spatially sparse precoding in millimeter wave mimo systems. *IEEE Transactions on Wireless Communications*, **13**(3), 1499–1513.

3. **Rappaport, T.**, **R. Heath**, **R. Daniels**, and **J. Murdock**, *Millimeter wave wireless communications*. Prentice Hall, 2015. ISBN 9780132172288.

4. **Xianghao, Y.** (2016). yuxianghao/alternating-minimization-algorithms-for-hybrid-precoding-in-millimeter-wave-mimo-systems. URL `https://github.com/yuxianghao`.

5. **Yu, X.**, **J.-C. Shen**, **J. Zhang**, and **K. B. Letaief** (2016). Alternating minimization algorithms for hybrid precoding in millimeter wave mimo systems. *IEEE Journal of Selected Topics in Signal Processing*, **10**(3), 485–500.

6. **Yu, X.**, **J. Zhang**, and **K. B. Letaief** (2018). A hardware-efficient analog network structure for hybrid precoding in millimeter wave systems. *IEEE Journal of Selected Topics in Signal Processing*, **12**(2), 282–297.

7. **Yu, X.**, **J. Zhang**, and **K. B. Letaief** (2019). Doubling phase shifters for efficient hybrid precoder design in millimeter-wave communication systems. *Journal of Communications and Information Networks*, **4**(2), 51.

8. **Zhang, J.**, **X. Yu**, and **K. B. Letaief** (2020). Hybrid beamforming for 5g and beyond millimeter-wave systems: A holistic view. *IEEE Open Journal of the Communications Society*, **1**, 77–91.